An Iterative Response-Surface-Based Approach for Chance-Constrained AC Optimal Power Flow Considering Dependent Uncertainty

Yijun Xu, *Member, IEEE*, Mert Korkali, *Senior Member, IEEE*, Lamine Mili, *Life Fellow, IEEE*, Jaber Valinejad, *Member, IEEE*, Tao Chen, *Member, IEEE*, and Xiao Chen

***Abstract*—A modern power system is characterized by a stochastic variation of the loads and an increasing penetration of renewable energy generation, which results in large uncertainties in its states. These uncertainties bring formidable challenges to the power system planning and operation process. To address these challenges, we propose a cost-effective, iterative response-surface-based approach for the chance-constrained AC optimal power-flow problem that aims to ensure the secure operation of the power systems considering dependent uncertainties. Starting from a stochastic-sampling-based framework, we first utilize the copula theory to simulate the dependence among multivariate uncertain inputs. Then, to reduce the prohibitive computational time required in the traditional Monte-Carlo method, we propose, instead of using the original complicated power-system model, to rely on a polynomial-chaos-based response surface. This response surface allows us to efficiently evaluate the time-consuming power-system model at arbitrary distributed sampled values with a negligible computational cost. This further enables us to efficiently conduct an online stochastic testing for the system states that not only screens out the statistical active constraints, but also assists in a better design of the tightened bounds without using any Gaussian or symmetric assumption. Finally, an iterative procedure is executed to fine-tune the optimal solution that better satisfies a predefined probability. The simulations conducted in multiple test systems demonstrate the excellent performance of the proposed method.**

***Index Terms*—AC optimal power flow, response surface, uncertainty, chance constraints, dependence.**

Manuscript received April 16, 2020; revised September 14, 2020; accepted January 7, 2021. Date of publication January 12, 2021; date of current version April 21, 2021. This work was supported in part by the U.S. National Science Foundation under Grant 1917308; in part by the United States Department of Energy Office of Electricity Advanced Grid Modeling (AGM) Program; and in part by the U.S. Department of Energy by Lawrence Livermore National Laboratory under Contract DE-AC52-07NA27344. Paper no. TSG-00568-2020. *(Corresponding authors: Yijun Xu; Tao Chen.)*

Yijun Xu, Lamine Mili, and Jaber Valinejad are with the Bradley Department of Electrical and Computer Engineering, Virginia Tech, Northern Virginia Center, Falls Church, VA 22043 USA (e-mail: yijunxu@vt.edu; lmili@vt.edu; jabervalinejad@vt.edu).

Mert Korkali is with the Computational Engineering Division, Lawrence Livermore National Laboratory, Livermore, CA 94550 USA (e-mail: korkali1@llnl.gov).

Tao Chen is with the Department of Electrical Engineering, Southeast University, Nanjing, China (e-mail: taoc@seu.edu.cn).

Xiao Chen is with the Center for Applied Scientific Computing, Lawrence Livermore National Laboratory, Livermore, CA 94550 USA (e-mail: chen73@llnl.gov).

Color versions of one or more figures in this article are available at https://doi.org/10.1109/TSG.2021.3051088.

Digital Object Identifier 10.1109/TSG.2021.3051088

I. Introduction

THE MODERN power system is inherently stochastic in nature. This is mainly due to the stochastic load variations over time and the intermittency of renewable energy resources. These uncertainties can bring formidable challenges to power system planning and operation. Ignoring them will produce inappropriate planning strategies or control actions, which, in turn, may result in system failures [1]. Therefore, recent research activities have focused on addressing the uncertainties in power system planning, monitoring, and control [1].

Since the traditional deterministic optimal power flow (OPF) faces the difficulties in handling the randomness of the input variables, the chance-constrained (CC)-AC-OPF has recently been advocated by many researchers as a viable method to tackle this optimization problem of decision making under uncertainty. Compared with the traditional deterministic approach, the CC approach restricts the feasible region with a predefined small probability to increase the confidence level of the solution [2], [3] and, therefore, is a relatively robust approach [4]. Compared with a fully robust approach, the CC approach provides a less conservative solution [5] to achieve a higher economic benefit. Therefore, the CC-AC-OPF provides a good balance between the economy and security in the power system operation [6].

In general, the CC-AC-OPF is a statistical problem considered to be difficult to solve. Some researchers prefer to use a sampling-based approach such as the Monte-Carlo (MC) method [7]. However, tens of thousands of MC simulations are typically required to achieve sufficiently accurate results, which is too time-consuming in practice. Some works in literature further adopt the scenario approach to reduce the computational burden of the MC method [8], [9], but sacrifice some level of accuracy [4]. Although its robust version based on a predefined robust sample set serves as a good candidate [6], [10], it may produce overconservative solution. Facing these difficulties in the sampling-based approach, many researchers advocate the analytic approaches for the capability of providing a closed-form solution that enables the CC-OPF problem applicable for the online application [10], [11]. However, due to the nonlinearity of the system model and the non-Gaussian distribution of the uncertainty, it is extremely difficult to derive an accurate closed-form solution. Most researchers simplified this problem by using a DC power-flow

1949-3053 © 2021 IEEE. Personal use is permitted, but republication/redistribution requires IEEE permission.
See https://www.ieee.org/publications/rights/index.html for more information.

Authorized licensed use limited to: to IEEExplore provided by University Libraries | Virginia Tech. Downloaded on May 20,2021 at 19:45:54 UTC from IEEE Xplore. Restrictions apply.

model [10], [11] while other researchers further improve this approach by incorporating a first-order linearization of the AC power-flow model [6], [12], [13]. Although this improved version shows excellent performance under the assumption that the forecast errors are very small [6], it provides inaccurate results when that assumption is violated in practice. Furthermore, to propagate the uncertainty in an analytical way, the uncertain inputs and outputs can be roughly modeled as a Gaussian distribution [6], [11].

Recently, some novel methods (e.g., generalized-polynomial-chaos (gPC) methods [14]) have been proposed for solving the CC-OPF problem. Using the gPC coefficients to obtain the first and the second statistical moments for the uncertain system states, this method has been applied in a DC-OPF model [15], and further extended to a AC-OPF model [16]. While this method does not have a linear assumption for the model and a Gaussian assumption for the uncertain inputs, its reformulation relies directly on the statistical moment provided by the gPC coefficients, under the assumption that all the uncertain inputs are independent and identically distributed (i.i.d.). A recent attempt has been made by Métivier *et al.* [17] to develop an iterative procedure in the polynomial chaos expansion (PCE) to avoid the statistical-moment-based reformulation and to enhance its scalability. However, the paper does not address the multidimensional dependence from uncertainties, nor does it consider any integration of renewable energy generation. We should emphasize that the independent assumption is typically violated in practice as it has been clearly demonstrated in various papers [18], [19]. This is mainly true for a power system with a high penetration of renewable energy resources [20]–[24]. Furthermore, only using the mean and variance to describe the statistical output implies a symmetric assumption for the uncertain system states. This assumption oversimplifies the statistical feature of the system states and is especially not true for the tail regions of the probability density functions (PDFs) [25]. Note that the statistical feature of the tail events should not be neglected since the CC-AC-OPF is oftentimes focused on the tail region of the density function with a small probability, e.g., 1%, 3%, 5%, and so on [6], [11], [13].

To overcome the aforementioned issues, this article proposes a novel iterative response-surface-based method for the CC-AC-OPF problem considering the dependent non-Gaussian uncertainties, resulting in the following contributions:

- To improve the computing efficiency of the uncertainty-propagation procedure within an MC framework, the response surfaces of the nonlinear AC power-flow model employ a PCE-based reduced-order representation.
- This response surface is merged into the copula theory to account for the dependence among high-dimensional uncertain inputs.
- The response-surface approach is used to efficiently conduct an online stochastic testing for detecting the statistical active constraints, which assists us in better designing the tightened bounds without the use of any Gaussian or symmetric assumption for the system states and the tail events.
- An iterative procedure is finally conducted to fine-tune the optimal solution for a better accuracy. Its amenability to parallel computation is also briefly discussed.

The performance of our proposed method has been analyzed through simulations that are carried out on the IEEE standard test system and a synthetic Illinois power system. These simulations reveal the excellent performance of the proposed method considering the simulation accuracy and the computing efficiency.

This article is organized as follows: in Section II, problem formulation is presented. In Section III, the background on response surface is provided. Section IV presents the proposed method. Case studies are presented in Section V while the conclusions and future work are provided in Section VI.

II. Problem Formulation

This section will first briefly summarize the deterministic AC-OPF model, and then extends it to the CC-AC-OPF model associated with the implementation challenges using the sampling-based approach.

A. Model Description of AC-OPF

Following Zhang and Li [2], we formulate the AC-OPF in power systems as

$$\min_{\mathbf{u}} \ f(\mathbf{x}, \mathbf{u}) \tag{1a}$$

$$\text{s.t.} \quad \mathbf{g}(\mathbf{x}, \mathbf{u}) = 0 \tag{1b}$$

$$\mathbf{h}_{\min} \le \mathbf{h}(\mathbf{x}, \mathbf{u}) \le \mathbf{h}_{\max} \tag{1c}$$

where $\mathbf{x} \in \mathbb{R}^N$ are vectors of dependent state variables, e.g., the voltage magnitude and angle at a PQ bus, the voltage angle and reactive power at a PV bus, the active and reactive power at the swing bus, and the power flow along the transmission lines; $\mathbf{u} \in \mathbb{R}^D$ are the vectors of the control variables, such as the generator power output and its voltage; f is a scalar objective function; and $\mathbf{g}$ and $\mathbf{h}$ are the vector-valued functions of equality and inequality constraints, respectively [2]. Typically, f is modeled as a quadratic cost function expressed as

$$f(\mathbf{x}, \mathbf{u}) = \sum_{i \in \mathcal{G}} \left(c_{2,i} P_{g,i}^2 + c_{1,i} P_{g,i} + c_{0,i} \right) \tag{2}$$

where c_2, c_1, and c_0 denote the cost coefficients; and $P_{g,i}$ denotes the power output of the ith conventional generator, which belongs to a set of $\mathcal{G}$. The equality constraints are described by a set of nonlinear power-flow equations for an N_b-bus system, which are given by

$$P_i = V_i \sum_{j=1}^{N_b} V_j \left(\mathbf{G}_{ij} \cos\theta_{ij} + \mathbf{B}_{ij} \sin\theta_{ij} \right) \tag{3a}$$

$$Q_i = V_i \sum_{j=1}^{N_b} V_j \left(\mathbf{G}_{ij} \sin\theta_{ij} - \mathbf{B}_{ij} \cos\theta_{ij} \right) \tag{3b}$$

where the net active and reactive power injection at Bus i are denoted by P_i and Q_i, respectively; the network conductance and susceptance matrix are denoted by $\mathbf{G}$ and $\mathbf{B}$, respectively;

Authorized licensed use limited to: to IEEExplore provided by University Libraries | Virginia Tech. Downloaded on May 20,2021 at 19:45:54 UTC from IEEE Xplore. Restrictions apply.

the voltage magnitude is denoted by V_i and the voltage angle difference between Buses i and j is given by θ_{ij}. The inequality constraints, $\mathbf{h}$, need to satisfy the vector-valued lower bound, $\mathbf{h}_{\min}$, and the vector-valued upper bound, $\mathbf{h}_{\max}$. Typically, they include some hard constraints due to the physical limits, such as the generator active power, $P_{g,i}$, and reactive power, $Q_{g,i}$, as well as some soft constraints, such as the current magnitudes of the transmission lines, which are denoted by I_{ij} [6]. They are described as

$$P_{g,i_{\min}} \le P_{g,i} \le P_{g,i_{\max}} \tag{4a}$$
$$Q_{g,i_{\min}} \le P_{g,i} \le Q_{g,i_{\max}} \tag{4b}$$
$$V_{i\min} \le V_i \le V_{i\max} \tag{4c}$$
$$I_{ij} \le I_{ij_{\max}}. \tag{4d}$$

Till now, we have formulated the AC-OPF model.

B. Model Enhancement via CC-AC-OPF

To account for the randomness of the loads and the renewable energy generation, it is easy to infer that we should reformulate the abovementioned AC-OPF functions into a stochastic form, such as $\mathbf{g}(\mathbf{x}, \mathbf{u}, \boldsymbol{\xi})$ and $\mathbf{h}(\mathbf{x}, \mathbf{u}, \boldsymbol{\xi})$, where $\boldsymbol{\xi} \in \mathbb{R}^S$ denotes a vector of random variables. However, it is very difficult to implement an optimization problem with random variables involved. To solve this problem, a traditional way is to reformulate this stochastic problem as a deterministic one by only considering the mean of the forecast random variables, $\mathbb{E}(\boldsymbol{\xi})$ [3], [6], where $\mathbb{E}$ is an expectation operator. Then, (1) can still be solved in a deterministic way via

$$\min_{\mathbf{u}} \ \sum_{i\in\mathcal{G}}\Big(c_{2,i}P_{g,i}^2 + c_{1,i}P_{g,i} + c_{0,i}\Big) \tag{5a}$$
$$\text{s.t.} \ \ \mathbf{g}(\mathbf{x}, \mathbf{u}, \mathbb{E}(\boldsymbol{\xi})) = 0 \tag{5b}$$
$$\mathbf{h}_{\min} \le \mathbf{h}(\mathbf{x}, \mathbf{u}, \mathbb{E}(\boldsymbol{\xi})) \le \mathbf{h}_{\max}. \tag{5c}$$

Albeit a simple strategy, the optimized solution is only a rough approximation that may lead to severe violations in the inequality constraints while its probability of the violation is not managed properly.

To precisely manage the violation rate for the optimized solution, the CC-AC-OPF model provides a much better alternative. By assigning a predefined probability to control the violation rate of the inequality constraints, $\mathbf{h}$, we formulate a CC-AC-OPF model as

$$\min_{\mathbf{u}} \ \sum_{i\in\mathcal{G}}\Big(c_{2,i}P_{g,i}^2 + c_{1,i}P_{g,i} + c_{0,i}\Big) \tag{6a}$$
$$\text{s.t.} \ \ \mathbf{g}(\mathbf{x}, \mathbf{u}, \boldsymbol{\xi}) = 0 \tag{6b}$$
$$\mathbb{P}(\mathbf{h}(\mathbf{x}, \mathbf{u}, \boldsymbol{\xi}) \in \mathcal{H}) \ge 1 - \boldsymbol{\epsilon} \tag{6c}$$

where $\mathcal{H}$ denotes a prescribed operational set determined by $\mathbf{h}_{\min}$ and $\mathbf{h}_{\max}$; and $\boldsymbol{\epsilon}$ denotes a vector of acceptable violation probability, which is typically set to be a small number (e.g., 1%, 5%, and 10%), to ensure a secure operation of the power systems. Note that the focus of this article is the individual chance-constrained problem, instead of a joint chance-constrained problem [13]. Therefore, for every individual set $\mathcal{H}_i$, (6c) can be decomposed as

$$\mathbb{P}(h_i(\mathbf{x}, \mathbf{u}, \boldsymbol{\xi}) \in \mathcal{H}_i) \ge 1 - \epsilon_i. \tag{7}$$

At this point, we have completed the formulation of the CC-AC-OPF.

C. Sampling-Based Approach and the Challenges Thereof

The most straightforward way to obtain the violation probability at its operation solution, $\mathbf{u}$, is the MC-based method [7], where a set of $N_{\boldsymbol{\xi}}$ samples are drawn from the multivariate probability distribution of $\boldsymbol{\xi}$, yielding $\{\boldsymbol{\xi}^{(j)}\}_{j=1}^{N_{\boldsymbol{\xi}}}$. Then, for each $\boldsymbol{\xi}^{(j)}$, $j = 1, \ldots, N_{\boldsymbol{\xi}}$, the equality constraint, $\mathbf{g}$, is evaluated at the sampled values, $\boldsymbol{\xi}^{(j)}$, to obtain the corresponding system states $\mathbf{x}^{(j)}$. Then, for every individual inequality constraint, we get

$$\mathbb{P}(h_i(\mathbf{x}, \mathbf{u}, \boldsymbol{\xi}) \in \mathcal{H}_i) = \sum_{j=1}^{N_{\boldsymbol{\xi}}} \frac{1}{N_{\boldsymbol{\xi}}} \chi_{\{\mathcal{H}_i\}}\Big(h_i\Big(\mathbf{x}^{(j)}, \mathbf{u}, \boldsymbol{\xi}^{(j)}\Big)\Big) \tag{8}$$

where χ is the characteristic function satisfying

$$\chi_{\{\mathcal{H}_i\}}(h_i(\mathbf{x}, \mathbf{u}, \boldsymbol{\xi})) = \begin{cases} 1 & \text{if } h_i(\mathbf{x}, \mathbf{u}, \boldsymbol{\xi}) \in \mathcal{H}_i \\ 0 & \text{if } h_i(\mathbf{x}, \mathbf{u}, \boldsymbol{\xi}) \notin \mathcal{H}_i. \end{cases} \tag{9}$$

Obviously, the computational burden of this MC method will be prohibitively heavy for a complicated power-system model. Notwithstanding that the violation probability can be obtained with the MC method, it is very difficult to guarantee that the obtained operation solution, $\mathbf{u}$, is a proper candidate to balance the security and economy in the OPF problem. If $\mathbf{u}$ is overconservative, then the violation probability evaluated through MC samples may be less than the predefined violation rate and therefore lose some economic benefits. Contrary to this, if the operation point, $\mathbf{u}$, is not conservative enough, then the MC-evaluated violation probability can be larger than the predefined ϵ. Here, the goal is to find a $\mathbf{u}$ that not only satisfies the chance constraints for the security objective, but also to provide a good economic performance.

III. Response-Surface-Based Sampling Approach

A. Motivation

To solve the abovementioned computational burden in the MC-based method for the CC-AC-OPF problem, we propose to use the response-surface method. For simplicity, let us first define a vector-valued nonlinear function $\mathbf{y}$ that combines the functions of $\mathbf{g}$ and $\mathbf{h}$. Then, we can use $\mathbf{y}$ to build a mapping between the uncertain random variables, $\boldsymbol{\xi}$, with the power system dependent variables, $\mathbf{x}$, at the fixed control variable, $\mathbf{u}$, expressed as

$$\mathbf{x} = \mathbf{y}(\boldsymbol{\xi}, \mathbf{u}). \tag{10}$$

Here, if we replace this complicated function $\mathbf{y} : \mathbb{R}^S \times \mathbb{R}^D \to \mathbb{R}^N$ with a simple functional form $\widetilde{\mathbf{y}}(\cdot)$ that captures the behavior of the complicated, high-fidelity simulation model of a power system while being computationally inexpensive to evaluate, then we call $\widetilde{\mathbf{y}}(\cdot)$ the response surface of

Authorized licensed use limited to: to IEEExplore provided by University Libraries | Virginia Tech. Downloaded on May 20,2021 at 19:45:54 UTC from IEEE Xplore. Restrictions apply.

TABLE I
UNIVARIATE GPC POLYNOMIAL BASES

Random Variable	Polynomial Basis Function	Support
Gaussian	Hermite	$(-\infty, +\infty)$
Gamma	Laguerre	$[0, +\infty)$
Beta	Jacobi	$[0, 1]$
Uniform	Legendre	$[-1, 1]$

the $\mathbf{y}(\cdot)$ [14], [19], [25]. It holds a relationship as $\widetilde{\mathbf{y}}(\boldsymbol{\xi}, \mathbf{u}) \approx \mathbf{y}(\boldsymbol{\xi}, \mathbf{u})$. This response surface enables us to accurately propagate a large amount of samples at negligible computing time and, therefore, can greatly enhance the computing efficiency of the sampling-based approach. Here, we choose the polynomial-chaos-expansion (PCE)-based response surface to mimic the power-system response under dependent uncertainty.

B. Review of the Generalized Polynomial Chaos Expansion

Introduced by Wiener and further developed by Xiu and Karniadakis [14], the generalized polynomial chaos expansion has been shown to be a cost-effective tool in modeling power-system response surfaces [19], [26], [27]. In the gPC method, the stochastic outputs are represented by a weighted sum of a given set of orthogonal polynomial chaos basis functions constructed from the probability distribution of the input random variables. For the vector of i.i.d. random variables, $\boldsymbol{\xi} = [\xi_1, \xi_2, \ldots, \xi_S]$, following a standard probability distribution (e.g., a Gaussian or the Beta distribution), to which, as shown in Table I [14], a unique orthogonal polynomial is associated. Let $\Phi_i(\xi_1, \xi_2, \ldots, \xi_S)$ denote this procedure's corresponding polynomial chaos basis and let a_i denote the ith polynomial chaos coefficient. For a stochastic system state, x, we have $x = \sum_{i=0}^{\infty} a_i \Phi_i(\boldsymbol{\xi})$. In practice, a truncated expansion is used such that

$$x = \sum_{i=0}^{S_P} a_i \Phi_i(\boldsymbol{\xi}) \tag{11}$$

where $S_P = (S+P)!/(S!P!) - 1$; S is the total number of the random variables involved in the gPC; and P is the maximum order of the polynomial chaos basis functions. It is found that a relatively low maximum polynomial chaos order (typically 2) provides output results with enough accuracy [19], [26]–[28]. From the polynomial chaos coefficients, the mean, μ, and the variance, σ^2, of the output x can be determined as

$$\mu = a_0 \tag{12}$$

$$\sigma^2 = \sum_{i=1}^{S_P} a_i^2 \mathbb{E}\left[\Phi_i^2\right]. \tag{13}$$

Remark 1: It is worth mentioning that although (12) and (13) build a straightforward connection between the polynomial chaos coefficients and the statistical moments, they are only valid under the i.i.d. assumption [5], [14], [29]. For the sake of completeness, a detailed proof and discussion of this property are provided in Appendix A. For some i.i.d.-assumption-based work, this property has successfully enabled a reformulation of the optimization problem [15], [16]. However, since we consider the dependence among multivariate uncertain inputs, for which i.i.d. is violated, (12) and (13) cannot be adopted in our approach. Here, we only use the response-surface feature of the gPC as described by (11).

1) The Orthogonal Polynomial Chaos Basis: A set of one-dimensional polynomial chaos basis functions $\{\Phi_i(\xi), i = 0, 1, 2, 3, \ldots\}$ with respect to some real positive measure satisfy

$$\int \Phi_i(\xi)\Phi_j(\xi)\mathrm{d}\lambda \begin{cases} = 0 & \text{if } i \neq j \\ > 0 & \text{if } i = j \end{cases} \tag{14}$$

where λ denotes a probability measure defined as the cumulative probability distribution function (CPDF) of ξ. For every CPDF, the associated orthogonal polynomials are unique.

2) Construction of the Polynomial Chaos Basis: A set of multidimensional polynomial chaos basis functions can be constructed as the tensor product of the one-dimensional polynomial chaos basis associated with each input random variable. Formally, we have

$$\Phi(\boldsymbol{\xi}) = \Phi(\xi_1) \otimes \Phi(\xi_2) \otimes \cdots \otimes \Phi(\xi_S) \tag{15}$$

where $\Phi(\xi_i)$ denotes the one-dimensional polynomial chaos basis for the ith random variable.

3) Collocation Points: To approximate the PCE coefficients, we evaluate the solver at a finite number of samples, typically in a small size. These finite samples are called the collocation points (CPs). The elements of the CPs are generated by using the union of the zeros and the roots of one higher-order, one-dimensional polynomial for every random variable [19], [30]. For example, starting from on-dimensional cases, for a 2nd-order Hermite polynomial, its one higher-order polynomial is $\phi_3(\xi) = \xi^3 - 3\xi$. The elements of the collocation points are $\sqrt{3}$,$-\sqrt{3}$, and 0. That means we need to evaluate the solver at the three sample points above to approximate the coefficients. In the multidimensional cases, the CPs are obtained by the tensor product of one-dimensional CPs. For examples, for the above 2nd-order Hermite polynomial with a dimension of 2, using tensor product, we get 9 combinations of the two-dimensional samples, i.e., $\{\sqrt{3}, \sqrt{3}\}$, $\{\sqrt{3}, 0\}$, $\{\sqrt{3}, -\sqrt{3}\}$, $\{0, \sqrt{3}\}$, $\{0, 0\}$, $\{0, -\sqrt{3}\}$, $\{-\sqrt{3}, \sqrt{3}\}$, $\{-\sqrt{3}, 0\}$, and $\{-\sqrt{3}, -\sqrt{3}\}$. More generally, if there are S random variables, the number of possible combinations is 3^S by using the tensor product. Therefore, the $S_P + 1$ unknown coefficients can be estimated at the selected CPs.

An improved version is the sparse-grid method [30]. Unlike the tensor-product rule that needs $(P+1)^S$ samples to simulate the forward solver, the sparse-grid method requires much fewer samples by using a sparse-tensor-product rule and, therefore, is considered in our approach.

IV. THE PROPOSED METHOD

In this section, we present the proposed iterative response-surface method to solve the CC-AC-OPF problem.

A. Dependence Modeling

The prerequisite of an uncertainty quantification relies on an precise uncertainty modeling. Here, we propose to model the

Authorized licensed use limited to: to IEEExplore provided by University Libraries | Virginia Tech. Downloaded on May 20,2021 at 19:45:54 UTC from IEEE Xplore. Restrictions apply.

dependence using copula technique since it can be perfectly merged into the framework of the response-surface method. According to Sklar's theorem, any joint multivariate cumulative distribution function $F_{\boldsymbol{\xi}}$ of an S-dimensional random vector can be expressed in terms of its marginal distributions and a copula to represent their dependence. Formally, we have

$$F_{\boldsymbol{\xi}}(\boldsymbol{\xi}) = C\big(F_{\xi_1}(\xi_1), F_{\xi_2}(\xi_2), \ldots, F_{\xi_S}(\xi_S)\big) \tag{16}$$

where $F_{\xi_i}(\xi_i)$ is the ith input marginal and $C(\cdot)$ is a copula that describes the dependence structure between the S-dimensional input variables [31]. Accordingly, its joint multivariate density function, $f_{\boldsymbol{\xi}}(\boldsymbol{\xi})$, can be obtained via

$$f_{\boldsymbol{\xi}}(\boldsymbol{\xi}) = c\big(F_{\xi_1}(\xi_1), \ldots, F_{\xi_S}(\xi_S)\big) \prod_{i=1}^{S} f_i(\xi_i) \tag{17}$$

where c is the S-variate copula density and $f_i(\xi_i)$ is the marginal density for the ith variable. Since there exist different copula families, such as the Archimedean copulae, the Gaussian copula and the vine copula, the choice of the copula function will influence the accuracy and computing efficiency of the dependence modeling. Here, we advocate the Gaussian copula for its simplicity and ability to generate high-dimensional dependent samples [32] while the Archimedean copulae (e.g., the Gumbel copula and the Frank copula) are not scalable because they are limited to the bivariate case [32], and the vine copula is very complicated and time-consuming for an online application [33].

B. Stochastic Testing via PCE and Copula

Here, the uncertainty parameters $\boldsymbol{m}$ for load and renewable power generation in the power-system model are viewed as random variables. By mapping the parameters $\boldsymbol{m}$ into $\boldsymbol{\xi}$, we can build a PCE as the response surface of power-flow solutions. The steps of the PCE procedure are detailed below:

(1) We construct the polynomial chaos basis with the Hermite polynomials. Then, we express the output x in the gPC expansion form of (11).

(2) We construct M_c combinations of collocation points, $\{\boldsymbol{\xi}^{(j)}\}_{j=1}^{M_c}$, and put them into an $M_c \times (S_P + 1)$ polynomial chaos basis matrix $\mathbf{H_{pc}}$. Formally, we have

$$\mathbf{H_{pc}} = \begin{bmatrix} \Phi_0(\boldsymbol{\xi}_1) & \Phi_1(\boldsymbol{\xi}_1) & \ldots & \Phi_{S_P}(\boldsymbol{\xi}_1) \\ \Phi_0(\boldsymbol{\xi}_2) & \Phi_1(\boldsymbol{\xi}_2) & \ldots & \Phi_{S_P}(\boldsymbol{\xi}_2) \\ \vdots & \vdots & \ddots & \vdots \\ \Phi_0(\boldsymbol{\xi}_{M_c}) & \Phi_1(\boldsymbol{\xi}_{M_c}) & \ldots & \Phi_{S_P}(\boldsymbol{\xi}_{M_c}) \end{bmatrix}. \tag{18}$$

(3) We map collocation points, $\{\boldsymbol{\xi}^{(j)}\}_{j=1}^{M_c}$ back to samples within actual physical space, i.e., $\{\boldsymbol{m}^{(j)}\}_{j=1}^{M_c}$. Following [19], for the jth collocation point at the ith random variable, this can be obtained via

$$m_i^{(j)} = F_i^{-1}\Big(T_i\Big(\xi_i^{(j)}\Big)\Big) \tag{19}$$

where F_i^{-1} is the inverse cumulative probability distribution function of m_i, and T_i is the cumulative probability distribution function of ξ_i. We would like to emphasize that this function is a well-known tool to provide mapping between different random variables, yet does not serve as a tool for *decorrelation*. For the readers' convenience, the statistical background of this transformation is provided in Appendix B, which is titled "Probability Integral Transform".

(4) By evaluating the aforementioned N-dimensional dependent variables, $\mathbf{x}$, through original power-system model $\mathbf{y}(\cdot)$ at the transformed collocation points $\{\boldsymbol{m}^{(j)}\}_{j=1}^{M_c}$, we obtain an $M_c \times N$ output matrix, $\mathbf{X}$.

(5) Estimate the unknown polynomial chaos coefficients matrix $\mathbf{A}$ based on the collocation points that are selected and the model output given by

$$\mathbf{X} = \mathbf{H_{pc}}\mathbf{A} \tag{20}$$

where $\mathbf{A}$ denotes an $(S_P + 1) \times N$ coefficient matrix expressed as

$$\mathbf{A} = \begin{bmatrix} a_{0,1} & a_{0,2} & \ldots & a_{0,N} \\ \vdots & \vdots & \ddots & \vdots \\ a_{S_P,1} & a_{S_P,2} & \ldots & a_{S_P,N} \end{bmatrix} \tag{21}$$

where $a_{i,j}$ denotes the ith PCE coefficient of the jth system state.

(6) Now, let $\hat{\mathbf{A}}$ be the coefficient matrix estimated using the weighted least-squares estimator [26], [29]. It is expressed as

$$\hat{\mathbf{A}} = \Big(\mathbf{H_{pc}^{\intercal}}\mathbf{H_{pc}}\Big)^{-1}\mathbf{H_{pc}^{\intercal}}\mathbf{X}. \tag{22}$$

With the coefficients matrix $\hat{\mathbf{A}}$, we obtain the response-surface form, $\widetilde{\mathbf{y}}(\boldsymbol{\xi}, \mathbf{u})$, for all the system states.

(7) Now, we can draw a large number of samples $\{\boldsymbol{\xi}^{(j)}\}_{j=1}^{N_{\boldsymbol{\xi}}}$ from the Gaussian copula and evaluate them through $\widetilde{\mathbf{y}}(\boldsymbol{\xi}, \mathbf{u})$ to obtain the system random output, $\{\mathbf{x}^{(j)}\}_{j=1}^{N_{\boldsymbol{\xi}}}$, at negligible computing time. For the readers' convenience, the step-by-step details of using the Gaussian copula to generate dependent samples are provided in Appendix C.

(8) Using the stochastic testing result, $\{\mathbf{x}^{(j)}\}_{j=1}^{N_{\boldsymbol{\xi}}}$, we directly compute the violation probability for each constraint via (7) and (8).

Remark 2: Note that since we use the Hermite polynomials, every ξ follows a Gaussian distribution. Even its associated "m" may follow other distributions, e.g., the Weibull distribution and the Beta distribution, we can conveniently use (19) to conduct an inverse CPDF transformation. This makes the response-surface-based method applicable to any probability distribution having a CPDF (or its PDF, of which we can take integral to obtain the corresponding CPDF as required in (19)).

To provide another way to interpret this conclusion, let us define a mapping between $\boldsymbol{\xi}$ and $\boldsymbol{m}$ as $\mathcal{T}$ to simplify (19) into

$$\boldsymbol{\xi} = \mathcal{T}(\boldsymbol{m}), \qquad \boldsymbol{m} = \mathcal{T}^{-1}(\boldsymbol{\xi}). \tag{23}$$

Then, (11) can be rewritten as

$$x = \sum_{i=0}^{S_P} a_i \Phi_i(\boldsymbol{\xi}) = \sum_{i=0}^{S_P} a_i \Phi_i(\mathcal{T}(\boldsymbol{m})) \tag{24}$$

Authorized licensed use limited to: to IEEExplore provided by University Libraries | Virginia Tech. Downloaded on May 20,2021 at 19:45:54 UTC from IEEE Xplore. Restrictions apply.

This transform enables us to use any type of input marginals, at the cost of an additional inverse CPDF transformation. We would also like to mention that if the nonlinearity in this transformation is very high (e.g., in the case of a multiple-peak distribution), the added nonlinearity may impact the accuracy of the PCE. Here, only single-peak distributions are considered in this article. We would also like to emphasize that by using the same inverse CPDF mapping strategy, good performances of the response-surface method in handling non-Gaussian distributions for the correlated renewables have been demonstrated in [19], [34], [35]. Therefore, we adopt this strategy here.

C. Reformulation of the Chance Constraints

Now, with the above stochastic testing results, we are able to reformulate the chance constraints given by (6c) as

$$\mathbf{h}_{\min} + \Delta\mathbf{h}_{\min} \le \mathbf{h}(\mathbf{x}, \mathbf{u}) \tag{25a}$$

$$\mathbf{h}(\mathbf{x}, \mathbf{u}) \le \mathbf{h}_{\max} - \Delta\mathbf{h}_{\max} \tag{25b}$$

which can be implemented as deterministic constraints using the optimization solver. In general, this reformulation involves an updating step to tighten the bounds. Here, $\Delta\mathbf{h}_{\min}$ and $\Delta\mathbf{h}_{\max}$ denote the non-negative, adjusted lower and upper margins, respectively. These tightened bounds will lead to a more conservative operation solution $\mathbf{u}$ at the expenses of a higher operating cost expressed in (2).

To design the updated margins that can not only ensure a predefined violation rate, ϵ_i, but also avoid an overconservative solution, let us first detect the active constraints. As addressed by Baker and Bernstein [13], in the optimization problem, the inactive constraints are those constraints, when removed, the optimal solution will not change while the active constraints are essential in determining the optimal solution. Besides, we further propose to incorporate the violation probability in classifying the active constraints. We define these statistical active constraints as constraints whose violation probabilities exceed the predefined violation rate. Let us consider the bus voltage magnitude V_i, bounded by [0.9, 1.1] pu. Suppose an $\epsilon = 5\%$ is predefined for its individual constraint, if the $\mathbb{P}(V_i \le 1.1) \le 95\%$, then we call it a "statistical active constraint," and vice versa. We only need to update these statistical active constraints and keep the statistical inactive constraint unchanged. For those classified as statistical active constraint, we calculate its updated margins through the quantile of its distributions via

$$\Delta h_{i\min} = Q(h_i, \mathbb{P}(h_i \in \mathcal{H}_i)) - Q(h_i, (1-\epsilon_i)) \tag{26a}$$

$$\Delta h_{i\max} = Q(h_i, (1-\epsilon_i)) - Q(h_i, \mathbb{P}(h_i \in \mathcal{H}_i)) \tag{26b}$$

where $Q(h_i, \mathbb{P})$ denotes the quantile value for the distribution of h_i at a probability value of $\mathbb{P}$. Obviously, for the inactive constraint, we have its $\Delta h_{i\min} = 0$ and $\Delta h_{i\max} = 0$. This quantile-based updating rule is chosen since it is based on an actual stochastic testing within the MC simulation framework [6] that can avoid the Gaussian or symmetric assumption of the system responses [11], [13], [16].

Here, we would like to emphasize that the Gaussian or symmetric assumptions may lead to an inaccurate margin adjustment. To illustrate this, we provide an example shown in Fig. 1. Let us take the power in a transmission line as an example. Suppose that its true nonparametric PDF is depicted in blue while its approximated Gaussian distribution with the same mean and variance is depicted in red. Assume that we have an upper bound set for this line as 31 MVA and a violation rate as 5%. As shown in Fig. 1, the PDF of the blue one is quite asymmetric and its 95% quantile goes beyond the limit of 31 MVA, which leads to a margin adjustment of $\Delta h_{\max}$. When it comes to the Gaussian-approximated red one, although it has some violations for the upper margin of 31 MVA, its 95% quantile is still located in the left side of the $h_{\max}$ with a violation probability smaller than 5%, which further implies this is not a statistical active constraint. Therefore, $\Delta h_{\max}$ is considered to be 0 for the red one. This example makes it obvious that a more general nonparametric PDF obtained from the sampling-based method provides a better choice than a simple Gaussian approximation.

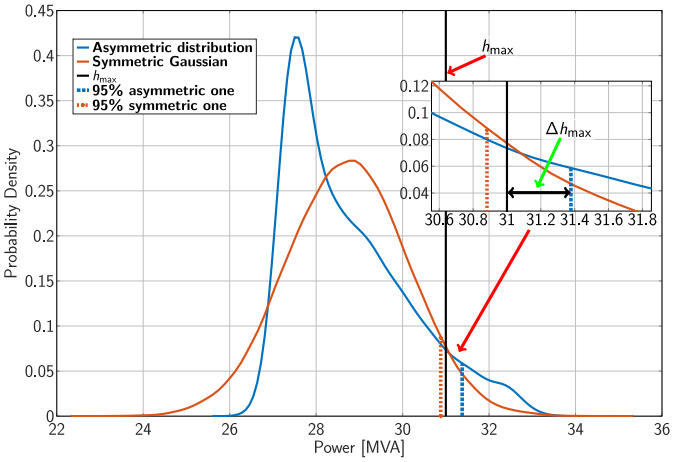

Fig. 1. Margin adjustment with the Gaussian assumption (red) and without the Gaussian assumption (blue).

D. The Iterative Procedure

Using the updated bounds, we can conduct a deterministic AC-OPF calculation using (5) to obtain an updated optimal solution $\mathbf{u}$. However, this is not the end of the algorithm since the updated operating solution, $\mathbf{u}$, may lead to some new statistical active constraints that necessitate further updating. Motivated by Roald and Anderson [6], who describe an iterative procedure that can improve the accuracy of the derivative-based method than a one-shot algorithm, we develop an iterative procedure to fine-tune our optimal solution. Now, let us define $\mathbf{u}^{(k)}$ as the optimal solution at the kth iteration. Then, for every updated $\mathbf{u}^{(k)}$, we further conduct a stochastic testing to check and update the statistical active constraints via $\Delta\mathbf{h}_{\min}^{(k)}$ and $\Delta\mathbf{h}_{\max}^{(k)}$ until the violation rate for each individual constraint can be satisfied. It should be emphasized that an iterative procedure is very rare in the sampling-based method because even one iteration is time-consuming; nonetheless, we can still complete the iterative procedure quite efficiently thanks to the PCE-based response surface. Also, note that, as Roald and Anderson have claimed in [6], while the iterative

Authorized licensed use limited to: to IEEExplore provided by University Libraries | Virginia Tech. Downloaded on May 20,2021 at 19:45:54 UTC from IEEE Xplore. Restrictions apply.

Algorithm 1 The Iterative Response-Surface-Based Approach for the CC-AC-OPF

1: Prepare the power-system model and its AC-OPF solver;
2: Prepare dependent sample set, $\{\mathbf{x}^{(j)}\}_{j=1}^{N_{\boldsymbol{\xi}}}$, via the Gaussian copula;
3: Generate collocation points, $\{\boldsymbol{\xi}^{(j)}\}_{j=1}^{M_c}$, and its transformed ones, $\{\boldsymbol{m}^{(j)}\}_{j=1}^{M_c}$;
4: Construct $\mathbf{H_{pc}}$ using polynomial chaos bases;
5: Set $k = 0$ and solve the deterministic AC-OPF via (5) to obtain an initial operating solution, $\mathbf{u}^{(0)}$;
6: **while** $k \leq k_{\max}$ **do**
7: At operating solution $\mathbf{u}^{(k)}$, evaluate the power-system response at collocation points to estimate the polynomial-chaos coefficients given by (20) via (22);
8: Conduct stochastic testing for system states via the response surface given by (11);
9: Detect the number of statistical active constraints, N_{ac};
10: **if** $N_{\text{ac}} > 0$ **then**
11: Update $k = k + 1$;
12: Update the constraint margin using $\Delta\mathbf{h}_{\min}^{(k)}$ and $\Delta\mathbf{h}_{\max}^{(k)}$ via (25) and (26);
13: Solve the deterministic AC-OPF via (5) with updated bounds to obtain the operating solution, $\mathbf{u}^{(k)}$;
14: **else**
15: **break** Jump to Step 18;
16: **end if**
17: **end while**
18: Read the CC-AC-OPF final solution, $\mathbf{u}^{(k)}$, and calculate the objective function.

procedure does not have a convergence guarantee, it can still preform well in practice. In this article, the algorithm converges in just a few iterations. Besides, we can also set a threshold, $k_{\max}$, as the maximum iteration number, e.g., 8 and 10. Now, we have concluded the presentation of the proposed iterative response-surface-based approach for the CC-AC-OPF problem. The summarized procedure is provided in Algorithm 1. It is also worth mentioning that most of the computing time of the response-surface method is spent on the training period, i.e., Step 7. Fortunately, this step can be executed in parallel.

V. Simulation Results

Using the proposed method, various case studies are conducted on the modified IEEE 30-bus test system [36] and a synthetic Illinois power system (i.e., the `ACTIVSg200` case) [37]. The algorithms are tested with the MATLAB R2018a version on a laptop with 2.60-GHz Intel Core i7-6600U processors and a 16 GB of main memory.

A. Demo Cases on the IEEE Standard Test System

In this part, we present some simple demo case studies conducted on the IEEE 30-bus system. Here, it is assumed that the loads follow a Gaussian distribution with mean values equal to the original bus loads and standard deviations equal to 5% of their means [19]. No renewable generation units are considered. We increase line capacities by 30%. Note that since we do not consider unit commitment in this article, the lower generation limits are set to zero as suggested by [6]. Besides, parallel computing is not utilized for this test system.

TABLE II
Validation on the Modified IEEE 30-Bus System

	$\boldsymbol{\epsilon} = 1\%$	$\boldsymbol{\epsilon} = 3\%$	$\boldsymbol{\epsilon} = 5\%$	$\boldsymbol{\epsilon} = 10\%$
$\epsilon_{\max}$	0.92%	3.08%	5.01%	9.71%
f	574.5518	574.5479	574.5458	574.5426
Time [s]	2.469	2.76	1.93	2.671

TABLE III
Validation on the Modified IEEE 30-Bus System

	$\delta = 5\%$	$\delta = 10\%$	$\delta = 15\%$
$\epsilon_{\max}$	5.01%	4.93%	4.81%
f	574.5458	574.5605	692.8025
Time [s]	1.93	1.84	4.1875

1) Validation of the Proposed Method: First, we test the performance of the proposed method under different acceptable violation probabilities, $\boldsymbol{\epsilon}$, using 10, 000 as the sample size. The simulation results of the proposed method are validated with the MC method with 10, 000 samples of power-flow cases to measure its maximum violation probability, $\epsilon_{\max}$, for each individual constraint. The simulation results are provided in Table II. It can be seen that the proposed method can provide an optimal solution with quite an accurate maximum violation probability, $\epsilon_{\max}$, under different predefined settings for $\boldsymbol{\epsilon}$. Moreover, the operation cost becomes slightly cheaper as the security level, indicated by $\boldsymbol{\epsilon}$, decreases. Finally, we can find that even with a sample size as large as 10, 000, without using parallel computing, the proposed method can finish simulation in less than 3 s. This demonstrates the accuracy and computing efficiency of the response-surface-based method.

2) Capability in Handling Different Levels of Nonlinearity: Now, we test the performance of the proposed method in handling different levels of nonlinearity. Here, we set the standard deviations of the load, δ, from 5% to 10% and 15% to increase the nonlinearity in the system as suggested in [6]. $\boldsymbol{\epsilon}$ is chosen as 5%. The other settings remain unchanged with the previous case. The simulation results are shown in Table III. It can be seen that even when the nonlinearity of the system increases, the proposed method can still provide accurate estimation results and the computing efficiency remains quite high. This is one of the advantages of the response-surface-based method since it has no linear assumption. Furthermore, as δ goes to 15%, the operating cost increases significantly to handle this randomness. Therefore, an accurate load forecast with a small level of uncertainty will greatly benefit the CC-AC-OPF solver in managing its operating cost.

B. Case Studies on an Illinois Power System

This case study is conducted on a synthetic 200-bus test case, fictitiously situated in the central part of the U.S. state of Illinois. In this test case with 200 buses, there are 49 generators

Authorized licensed use limited to: to IEEExplore provided by University Libraries | Virginia Tech. Downloaded on May 20,2021 at 19:45:54 UTC from IEEE Xplore. Restrictions apply.

TABLE IV
CORRELATION MATRIX OF THE INPUTS

	Load	**W 1**	**W 2**	**W 3**	**W 4**
Load	1	0.5	0.3	0.5	0.6
W 1	0.5	1	0.7	0.8	0.6
W 2	0.3	0.7	1	0.8	0.5
W 3	0.5	0.8	0.8	1	0.4
W 4	0.6	0.6	0.5	0.4	1

TABLE V
VALIDATION OF THE PROPOSED METHOD WITH DIFFERENT SAMPLE SIZES UNDER DIFFERENT ACCEPTABLE VIOLATION PROBABILITIES

Group 1 **using** $\epsilon = 3\%$					
Samples	Iterations	Time [s]	$f_{\text{ite}}[\$]$	$f_{\text{os}}[\$]$	$\epsilon_{\max}[\%]$
1,000	5	6.87	32,116	31,936	5.2
5,000	5	9.09	32,107	31,891	3.21
10,000	5	10.45	32,128	31,919	3.12
Group 2 **using** $\epsilon = 5\%$					
Samples	Iterations	Time [s]	$f_{\text{ite}}[\$]$	$f_{\text{os}}[\$]$	$\epsilon_{\max}[\%]$
1,000	6	10.328	31,781	31,683	6.28
5,000	7	11.59	31,847	31,745	5.07
10,000	6	11.16	31,837	31,726	5.03
Group 3 **using** $\epsilon = 10\%$					
Samples	Iterations	Time [s]	$f_{\text{ite}}[\$]$	$f_{\text{os}}[\$]$	$\epsilon_{\max}[\%]$
1,000	3	4.2	31,402	31,402	12.21
5,000	4	7.813	31,453	31,453	9.96
10,000	3	6.33	31,469	31,469	9.99
Group 4 **using** $\epsilon = 15\%$					
Samples	Iterations	Time [s]	$f_{\text{ite}}[\$]$	$f_{\text{os}}[\$]$	$\epsilon_{\max}[\%]$
1,000	3	3.4375	31,228	31,228	17.58
5,000	3	5.1563	31,283	31,283	15.32
10,000	3	5.7656	31,293	31,293	14.84

in total. For the associated PV buses, their voltage magnitudes and generated power outputs are considered as control variables. Here, it is assumed that the loads follow a Gaussian distribution with mean values equal to the original bus loads and standard deviations equal to 5% of their means. 4 wind farms, each with a rated power of 50 MW, are added at Buses 5, 15, 100, and 140, respectively, to introduce the randomness in the OPF model. Their shape and scale parameters are set to {7.41, 2.06} [19]. Their correlation matrix of these dependent inputs is provided in Table IV. The Gaussian copula is used to model the dependent samples. The generation limits are increased by a factor of 1.3 and unit commitment is not considered. Besides, we further merge the parallel computing into the proposed method as described in Section IV-D.

1) Validation of the Proposed Method: First, we test the performance of the proposed method under different sample sizes and different acceptable violation probabilities, $\boldsymbol{\epsilon}$. The simulation results of the proposed method are validated with the MC method with 10,000 samples of power-flow cases to measure its maximum violation probability, $\epsilon_{\max}$, for all the individual constraints. We also compare the solution of the proposed iterated method, f_{ite}, with that of the one-shot method, f_{os}, which does not have an iterative procedure. The simulation results are demonstrated in Table V.

From Table V, the following conclusions can be drawn:

- The operating cost, $f_{\text{ite}}[\$]$, will increase with a smaller $\boldsymbol{\epsilon}$. This is the tradeoff between the security and the economy. Furthermore, compared to the solution of \$30,547 obtained via a deterministic method formulated in (5), the proposed method can always provide a more conservative result.
- Considering the validated maximum violation probability, $\epsilon_{\max}[\%]$, under the MC method, we have found that with 5,000 samples, the proposed method can ensure quite an accurate simulation result in the presence of dependent uncertain inputs.
- In spite of using an iterative-sampling-based procedure, the proposed method can still complete the simulation in just a few seconds on a personal laptop with the execution of parallel computing. The number of iterations is, in general, just a few. Considering that the redispatch interval in a power system may include 5, 10, or 15 min, etc., [8], the computing efficiency of the proposed method has already been excellent enough for an online application.
- The performance of the proposed method depends on the choice of a proper sample size. A small sample size, such as 1,000, may lead to relatively inaccurate violation probabilities of the sampling-based method. This is especially true for some small probability, such as 3% and 5%. In general, 5,000 is required to ensure an accurate violation probability. Fortunately, thanks to the response surface, we have found that the computing time is still very small even under 10,000 sample size.
- For a relatively large value of $\epsilon_{\max}$, such as 10% and 15%, there is no obvious difference between the solutions of the iterative method and the one-shot method. However, when it comes to the tail events associated with a small probability, such as 3% and 5%, the iterative method provides a more conservative result in the objective function and ensures an accurate violation probability.

2) Approximation Accuracy of the PCE-Based Response Surface: Here, we would like to emphasize that the accuracy of the proposed method highly depends on the accuracy of the approximation of the PCE-based response surface since it is the foundation of the proposed method. As we have briefly mentioned in Section III-B, a PCE of order 2 is a popular choice; therefore, we choose this setting for all the experiments in the article. As examples, let us choose the voltage magnitude on the Bus 20 and the power on Line 240 as the quantities of interest (QoIs). Using the operation solutions obtained through the experiment settings defined in Groups 1, 2, 3, and 4 as shown in Table V, we validate the accuracy of the PCE-based response surface through its obtained PDFs for these QoIs, which are further compared to the simulation results obtained by the MC method, with 10,000 samples as a reasonable benchmark. The simulation results are shown in Fig. 2. It can be seen that, for all the above test conditions, the PCE-based response surface of order 2 can provide quite accurate simulation results under dependent random inputs. This validates the accuracy of the PCE-based surrogate of order 2 and accords with the conclusion reached in other similar bodies of work in [5], [16], [19], [25], [27]–[29]. We do not suggest a higher order of the PCE due to the "curse

Authorized licensed use limited to: to IEEExplore provided by University Libraries | Virginia Tech. Downloaded on May 20,2021 at 19:45:54 UTC from IEEE Xplore. Restrictions apply.

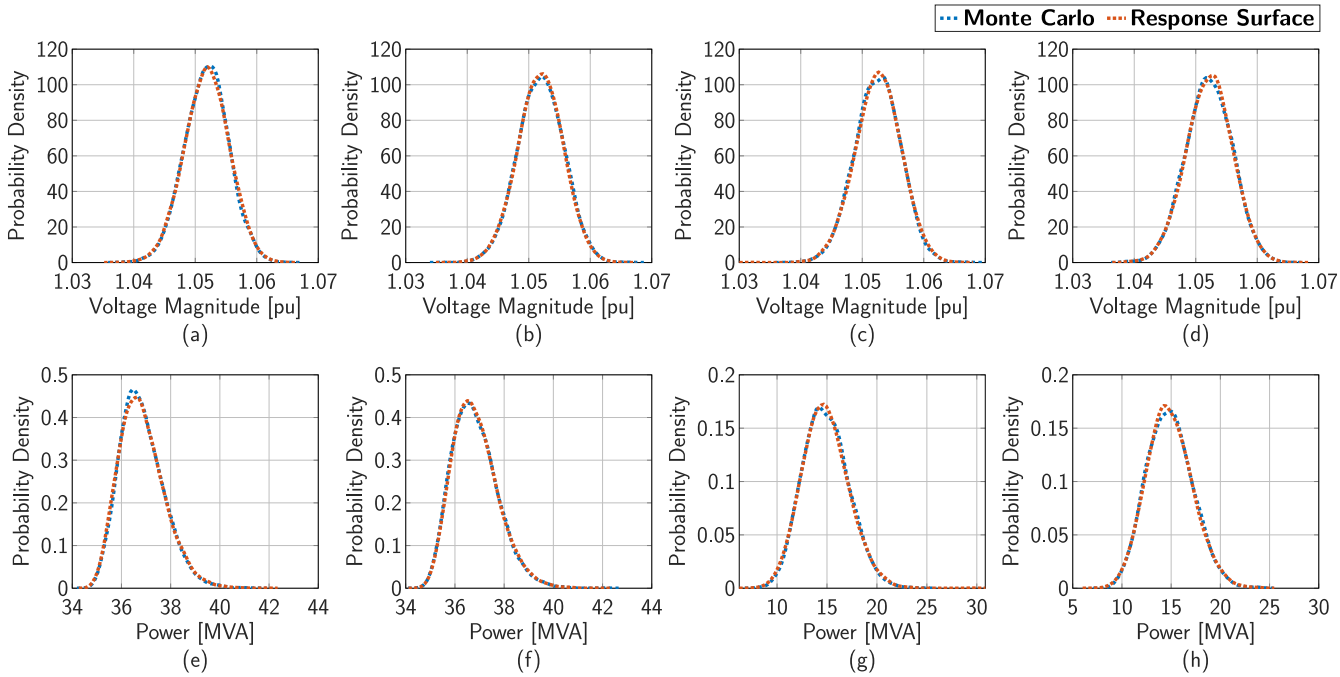

Fig. 2. PDFs of (a) voltage magnitude at Bus 20 under Group 1 setting; (b) voltage magnitude at Bus 20 under Group 2 setting; (c) voltage magnitude at Bus 20 under Group 3 setting; (d) voltage magnitude at Bus 20 under Group 4 setting; (e) power on Line 240 under Group 1 setting; (f) power on Line 240 at Bus 20 under Group 2 setting; (g) power on Line 240 at Bus 20 under Group 3 setting; (h) power on Line 240 at Bus 20 under Group 4 setting.

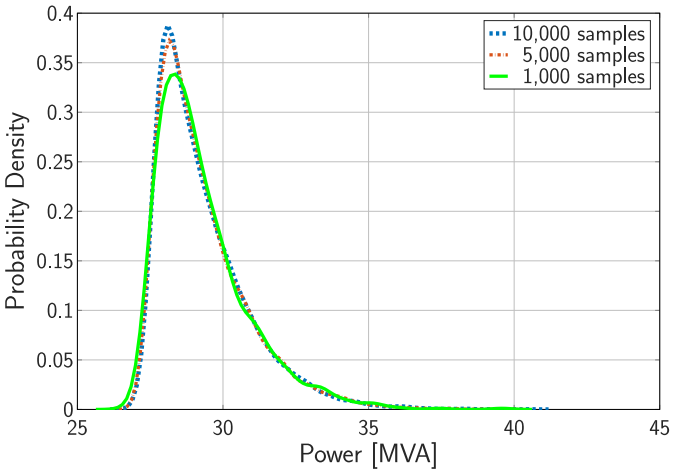

Fig. 3. PDFs of P_{232} using different sample size.

of dimensionality" [30] while providing little improvement in accuracy [27], [38]. Besides, a lower order (i.e., 1) is also not suggested since it has been shown to be not sufficiently accurate for power system applications in [17], [39].

3) Discussion on the Symmetry: Here, let us discuss the symmetric assumption for the system states that are widely adopted in the literature. Let us choose the power on Line 232, P_{232}, as an example. Here, we plot its PDFs obtained with $1,000$, $5,000$, and $10,000$ samples in Fig. 3. It can be seen that the PDFs are quite asymmetric with a long tail on the potential violation region. Using a symmetric assumption or simply using a Gaussian distribution with the same mean and variance to approximate it may lead to quite inaccurate estimation results. This is the advantage of the sampling-based method which only needs to use the quantile function, Q, to give it a general estimation.

TABLE VI
ACCURACY OF THE TAILS

	$\epsilon = 3\%$	$\epsilon = 5\%$	$\epsilon = 10\%$
$\mid Q_{1k} - Q_{10k} \mid$ [MVA]	0.2404	0.0578	0.0179
$\mid Q_{5k} - Q_{10k} \mid$ [MVA]	0.0512	0.0053	0.0116

4) Accuracy of the Tails: From Fig. 3, we can also see that although the PDF obtained by $1,000$ samples is not as accurate as those obtained by a larger number of samples, such as $5,000$, its entire approximation of the PDF is still reasonable. However, if we further go to the tail events, this becomes a more complicated case [25]. Let us compare the quantile values obtained with $1,000$ samples, Q_{1k}, and $5,000$ samples, Q_{5k} to the benchmark results obtained by $10,000$ samples, Q_{10k}, as shown in Table VI. It can be seen that using samples of size $1,000$, the errors in the quantile increase significantly as ϵ becomes smaller while errors in the quantile obtained by samples of size $5,000$ can provide a more accurate and stable estimation for a relatively smaller ϵ. This means that the sample size for the sampling-based method should be well-designed for different acceptable violation probabilities. For tail events located in the small-probability region, the sample size should be increased to maintain accuracy. Fortunately, the response-surface method can efficiently propagate a large number of samples as demonstrated by the experiments above.

VI. Conclusion and Future Work

In this article, we propose an iterative response-surface-based approach to solve the CC-AC-OPF problem. Using the

Authorized licensed use limited to: to IEEExplore provided by University Libraries | Virginia Tech. Downloaded on May 20,2021 at 19:45:54 UTC from IEEE Xplore. Restrictions apply.

PCE-based response surface, we can efficiently evaluate a large amount of dependent samples to estimate the violation probability for each individual constraint. This allows us to properly reformulate the optimization problem with a more conservative solution. The simulation results have demonstrated the excellent performances of the proposed method from the standpoint of accuracy and efficiency.

In the future, we will further improve the scalability of the proposed method since the polynomial chaos expansion suffers from the "curse of dimensionality" when the number of the random variables goes very high. To this end, we will investigate some emerging techniques, e.g., the sparse polynomial chaos [29] and the polynomial-chaos ANOVA [39], to further ameliorate the performance of the proposed method in solving very-large-dimensional problems.

APPENDIX A
STATISTICS FOR POLYNOMIAL CHAOS EXPANSIONS

Here, let us prove (12) and (13) under the i.i.d. assumption. First, following the definition, to calculate the mean value for the PCE, $x = \sum_{i=0}^{S_P} a_i \Phi_i(\boldsymbol{\xi})$, we get

$$\mu = \mathbb{E}[x] = \int \sum_{i=0}^{S_P} a_i \Phi_i(\boldsymbol{\xi}) f_{\boldsymbol{\xi}}(\boldsymbol{\xi})\, \mathrm{d}\boldsymbol{\xi} \tag{A.1}$$

Based on (15), we have $\Phi_0(\boldsymbol{\xi}) = 1$. Then, (11) is rewritten as

$$x = a_0 + \sum_{i=1}^{S_P} a_i \Phi_i(\boldsymbol{\xi}). \tag{A.2}$$

This transform (A.1) as

$$\begin{aligned}\mu &= a_0 \int f_{\boldsymbol{\xi}}(\boldsymbol{\xi})\, \mathrm{d}\boldsymbol{\xi} + \sum_{i=1}^{S_P} \int a_i \Phi_i(\boldsymbol{\xi}) f_{\boldsymbol{\xi}}(\boldsymbol{\xi})\, \mathrm{d}\boldsymbol{\xi} \\ &= a_0 + \sum_{i=1}^{S_P} a_i \int \Phi_i(\boldsymbol{\xi}) f_{\boldsymbol{\xi}}(\boldsymbol{\xi})\, \mathrm{d}\boldsymbol{\xi}. \end{aligned} \tag{A.3}$$

Here, for the second term in (A.3), we have

$$\Phi_i(\boldsymbol{\xi}) = \prod_{k=1}^{S} \Phi_{k,i_k}(\xi_k) \tag{A.4}$$

where $\Phi_{k,i_k}(\xi_k)$ is a univariate degree-i_k orthogonal polynomial of a random variable ξ_k [40]. Consequently, if and only if $\{\xi_1, \xi_2, \ldots, \xi_S\}$ are mutually independent, we have

$$f_{\boldsymbol{\xi}} = \prod_{i=1}^{S} f_i(\xi_i) \tag{A.5}$$

Till now, due to the orthogonality property between the terms in (A.4) and (A.5), $\sum_{i=1}^{S_P} a_i \int \Phi_i(\boldsymbol{\xi}) f_{\boldsymbol{\xi}}(\boldsymbol{\xi})\, \mathrm{d}\boldsymbol{\xi} = 0$. We have $\mu = a_0$, as (12) shows.

Based on this, using the definition of the variance, we have

$$\sigma^2 = \mathbb{E}\left[\left(\sum_{i=0}^{S_P} a_i \Phi_i(\boldsymbol{\xi}) - \mu\right)^2\right]. \tag{A.6}$$

Using (A.2) and (12), (A.6) is rewritten as

$$\sigma^2 = \mathbb{E}\left[\left(\cancel{a_0} + \sum_{i=1}^{S_P} a_i \Phi_i(\boldsymbol{\xi}) - \cancel{a_0}\right)^2\right] = \sum_{i=1}^{S_P} a_i^2\, \mathbb{E}\left[\Phi_i^2\right]. \tag{A.7}$$

Now, the proof is completed for (12) and (13) under i.i.d. assumptions.

Remark 3: Obviously, for the dependent random variable cases, (A.5) no longer holds. To decompose the joint density function into the marginal ones, we have to incorporate the copula functions via $f_{\boldsymbol{\xi}}(\boldsymbol{\xi}) = c(F_{\xi_1}(\xi_1), \ldots, F_{\xi_S}(\xi_S)) \prod_{i=1}^{S} f_i(\xi_i)$ as shown in (17). Then, each term in the second part of (A.3) can be represented by $a_i \int \Phi_i(\boldsymbol{\xi}) c(F_{\xi_1}(\xi_1), \ldots, F_{\xi_S}(\xi_S)) \prod_{i=1}^{S} f_i(\xi_i)\, \mathrm{d}\boldsymbol{\xi}$. Due to the incorporation of nonlinear copula functions, orthogonality no longer holds. Consequently, (12) does not hold for this dependent random input case. Subsequently, (13) cannot hold either.

APPENDIX B
PROBABILITY INTEGRAL TRANSFORM

Let us provide some basic background of the probability theory used in (19). It is well-known that for any random variable ξ with a continuous CPDF F_ξ, the random variable

$$U = F_\xi(\xi) \tag{B.1}$$

follows a uniform distribution as $U \sim \mathcal{U}[0, 1]$. This is also called the probability integral transform of ξ [41]. Its inverse mapping can be obtained via

$$\xi = F_\xi^{-1}(U) \tag{B.2}$$

to map the $U \sim \mathcal{U}[0, 1]$ into $\xi \sim F_\xi$. This probability integral transform and its inverse mapping are the foundation of the inverse CPDF mapping used in (19), which maps a random variable from the physical space to a standard Gaussian space, and vice versa.

APPENDIX C
GAUSSIAN COPULA

Let us present how to simulate dependent samples with the Gaussian copula. All the details here follow Mai and Scherer of [32, Ch. 4]. To simulate a random vector from the Gaussian copula, C_P^{Gauss}, where $P \in \mathbb{R}^{S \times S}$ is a positive-definite correlation matrix, we conduct the following steps:

1) Compute the Cholesky decomposition of P with $LL^\intercal = P$, where $L \in \mathbb{R}^{S \times S}$ is a lower triangular matrix.
2) Simulate a vector of independent standard normal random variables with $\boldsymbol{Z} \in \mathcal{N}_S(\boldsymbol{0}, \boldsymbol{I})$.
3) Compute $\boldsymbol{X}^r = L\boldsymbol{Z} \in \mathcal{N}_S(L\boldsymbol{0}, L\boldsymbol{I}L^\intercal) = \mathcal{N}_S(\boldsymbol{0}, P)$.
4) Return the vector of $[F(X_1^r), \ldots, F(X_S^r)]^\intercal$, where F is the distribution function of a univariate standard normal distribution.

Once we obtain the Gaussian copula, we can easily use the abovementioned inverse CPDF function to conduct a mapping between different types of random variables. This is also known as the Nataf transformation as illustrated in [42], [43].

Authorized licensed use limited to: to IEEExplore provided by University Libraries | Virginia Tech. Downloaded on May 20,2021 at 19:45:54 UTC from IEEE Xplore. Restrictions apply.

REFERENCES

[1] M. Schwalbe, *Mathematical Sciences Research Challenges for the Next-Generation Electric Grid: Summary of a Workshop (ser. National Academies of Sciences, Engineering, and Medicine)*. Washington, DC, USA: Nat. Acad. Press, 2015.

[2] H. Zhang and P. Li, "Chance constrained programming for optimal power flow under uncertainty," *IEEE Trans. Power Syst.*, vol. 26, no. 4, pp. 2417–2424, Nov. 2011.

[3] G. Li and X. Zhang, "Stochastic optimal power flow approach considering correlated probabilistic load and wind farm generation," in *Proc. IET Conf. Rel. Transm. Distrib. Netw.*, Nov. 2011, pp. 773–781.

[4] M. Lubin, Y. Dvorkin, and S. Backhaus, "A robust approach to chance constrained optimal power flow with renewable generation," *IEEE Trans. Power Syst.*, vol. 31, no. 5, pp. 3840–3849, Sep. 2016.

[5] C. Cui, K. Liu, and Z. Zhang, "Chance-constrained and yield-aware optimization of photonic ICs with non-Gaussian correlated process variations," *IEEE Trans. Comput.-Aided Design Integr. Circuits Syst.*, vol. 39, no. 12, pp. 4958–4970, Dec. 2020.

[6] L. Roald and G. Andersson, "Chance-constrained AC optimal power flow: Reformulations and efficient algorithms," *IEEE Trans. Power Syst.*, vol. 33, no. 3, pp. 2906–2918, May 2018.

[7] H. Zhang and P. Li, "Probabilistic analysis for optimal power flow under uncertainty," *IET Gener. Transm. Distrib.*, vol. 4, no. 5, pp. 553–561, May 2010.

[8] M. Vrakopoulou, B. Li, and J. L. Mathieu, "Chance constrained reserve scheduling using uncertain controllable loads part I: Formulation and scenario-based analysis," *IEEE Trans. Smart Grid*, vol. 10, no. 2, pp. 1608–1617, Mar. 2019.

[9] K. Margellos, P. Goulart, and J. Lygeros, "On the road between robust optimization and the scenario approach for chance constrained optimization problems," *IEEE Trans. Autom. Control*, vol. 59, no. 8, pp. 2258–2263, Aug. 2014.

[10] Y. Zhang, S. Shen, and J. L. Mathieu, "Distributionally robust chance-constrained optimal power flow with uncertain renewables and uncertain reserves provided by loads," *IEEE Trans. Power Syst.*, vol. 32, no. 2, pp. 1378–1388, Mar. 2017.

[11] B. Li, M. Vrakopoulou, and J. L. Mathieu, "Chance constrained reserve scheduling using uncertain controllable loads part II: Analytical reformulation," *IEEE Trans. Smart Grid*, vol. 10, no. 2, pp. 1618–1625, Mar. 2019.

[12] E. Dall'Anese, K. Baker, and T. Summers, "Chance-constrained AC optimal power flow for distribution systems with renewables," *IEEE Trans. Power Syst.*, vol. 32, no. 5, pp. 3427–3438, Sep. 2017.

[13] K. Baker and A. Bernstein, "Joint chance constraints in AC optimal power flow: Improving bounds through learning," *IEEE Trans. Smart Grid*, vol. 10, no. 6, pp. 6376–6385, Nov. 2019.

[14] D. Xiu and G. E. Karniadakis, "The Wiener–Askey polynomial chaos for stochastic differential equations," *SIAM J. Sci. Comput.*, vol. 24, no. 2, pp. 619–644, 2002.

[15] T. Mühlpfordt, T. Faulwasser, L. Roald, and V. Hagenmeyer, "Solving optimal power flow with non-Gaussian uncertainties via polynomial chaos expansion," in *Proc. IEEE Conf. Decis. Control*, Dec. 2017, pp. 4490–4496.

[16] T. Mühlpfordt, L. Roald, V. Hagenmeyer, T. Faulwasser, and S. Misra, "Chance-constrained AC optimal power flow: A polynomial chaos approach," *IEEE Trans. Power Syst.*, vol. 34, no. 6, pp. 4806–4816, Nov. 2019.

[17] D. Métivier, M. Vuffray, and S. Misra, "Efficient polynomial chaos expansion for uncertainty quantification in power systems," in *Proc. Power Syst. Comput. Conf.*, Jul. 2020, pp. 1–6. [Online]. Available: http://pscc.epfl.ch/rms/modules/request.php?module=oc_program&action=view.php&id=993&file=1/993.pdf

[18] G. Papaefthymiou and D. Kurowicka, "Using copulas for modeling stochastic dependence in power system uncertainty analysis," *IEEE Trans. Power Syst.*, vol. 24, no. 1, pp. 40–49, Feb. 2009.

[19] Z. Ren, W. Li, R. Billinton, and W. Yan, "Probabilistic power flow analysis based on the stochastic response surface method," *IEEE Trans. Power Syst.*, vol. 31, no. 3, pp. 2307–2315, May 2016.

[20] F. Qiu and J. Wang, "Chance-constrained transmission switching with guaranteed wind power utilization," *IEEE Trans. Power Syst.*, vol. 30, no. 3, pp. 1270–1278, May 2015.

[21] M. Vrakopoulou, K. Margellos, J. Lygeros, and G. Andersson, "A probabilistic framework for reserve scheduling and N−1 security assessment of systems with high wind power penetration," *IEEE Trans. Power Syst.*, vol. 28, no. 4, pp. 3885–3896, Nov. 2013.

[22] Z. Hu *et al.*, "Uncertainty quantification in stochastic economic dispatch using Gaussian process emulation," in *Proc. IEEE PES Innov. Smart Grid Tech. Conf*, Feb. 2020, pp. 1–5.

[23] Y. Xu *et al.*, "A data-driven nonparametric approach for probabilistic load-margin assessment considering wind power penetration," *IEEE Trans. Power Syst.*, vol. 35, no. 6, pp. 4756–4768, Nov. 2020.

[24] Z. Hu *et al.*, "A Bayesian approach for estimating uncertainty in stochastic economic dispatch considering wind power penetration," *IEEE Trans. Sustain. Energy*, vol. 12, no. 1, pp. 671–681, Jan. 2021.

[25] Y. Xu, M. Korkali, L. Mili, X. Chen, and L. Min, "Risk assessment of rare events in probabilistic power flow via hybrid multi-surrogate method," *IEEE Trans. Smart Grid*, vol. 11, no. 2, pp. 1593–1603, Mar. 2020.

[26] Y. Xu *et al.*, "Response-surface-based Bayesian inference for power system dynamic parameter estimation," *IEEE Trans. Smart Grid*, vol. 10, no. 6, pp. 5899–5909, Nov. 2019.

[27] E. Haesen, C. Bastiaensen, J. Driesen, and R. Belmans, "A probabilistic formulation of load margins in power systems with stochastic generation," *IEEE Trans. Power Syst.*, vol. 24, no. 2, pp. 951–958, May 2009.

[28] C. Safta, R. L.-Y. Chen, H. N. Najm, A. Pinar, and J.-P. Watson, "Efficient uncertainty quantification in stochastic economic dispatch," *IEEE Trans. Power Syst.*, vol. 32, no. 4, pp. 2535–2546, Jul. 2017.

[29] F. Ni, P. H. Nguyen, and J. F. G. Cobben, "Basis-adaptive sparse polynomial chaos expansion for probabilistic power flow," *IEEE Trans. Power Syst.*, vol. 32, no. 1, pp. 694–704, Jan. 2017.

[30] D. Xiu, *Numerical Methods for Stochastic Computations: A Spectral Method Approach*. Upper Saddle River, NJ, USA: Princeton Univ. Press, 2010.

[31] R. B. Nelsen, *An Introduction to Copulas*. New York, NY, USA: Springer, 2007.

[32] J.-F. Mai and M. Scherer, *Simulating Copulas: Stochastic Models, Sampling Algorithms, and Applications*, 2nd ed. Singapore: World Sci., 2017.

[33] Z. Wang, W. Wang, C. Liu, Z. Wang, and Y. Hou, "Probabilistic forecast for multiple wind farms based on regular vine copulas," *IEEE Trans. Power Syst.*, vol. 33, no. 1, pp. 578–589, Jan. 2018.

[34] X. Xu, Z. Yan, M. Shahidehpour, H. Wang, and S. Chen, "Power system voltage stability evaluation considering renewable energy with correlated variabilities," *IEEE Trans. Power Syst.*, vol. 33, no. 3, pp. 3236–3245, May 2018.

[35] X. Fu, Q. Guo, and H. Sun, "Statistical machine learning model for stochastic optimal planning of distribution networks considering a dynamic correlation and dimension reduction," *IEEE Trans. Smart Grid*, vol. 11, no. 4, pp. 2904–2917, Jul. 2020.

[36] *University of Washington, Power Systems Test Case Archive*. Accessed: Sep. 2020. [Online]. Available: https://labs.ece.uw.edu/pstca/

[37] *Electric Grid Test Case Repository, Illinois 200-Bus System: ACTIVSg200*. Accessed: Sep. 2020. [Online]. Available: http://electricgrids.engr.tamu.edu/electric-grid-test-cases/activsg200/

[38] Y. Xu, L. Mili, M. Korkali, and X. Chen, "An adaptive Bayesian parameter estimation of a synchronous generator under gross errors," *IEEE Trans. Ind. Informat.*, vol. 16, no. 8, pp. 5088–5098, Aug. 2020.

[39] Y. Xu, L. Mili, and J. Zhao, "Probabilistic power flow calculation and variance analysis based on hierarchical adaptive polynomial chaos-ANOVA method," *IEEE Trans. Power Syst.*, vol. 34, no. 5, pp. 3316–3325, Sep. 2019.

[40] C. Cui and Z. Zhang, "High-dimensional uncertainty quantification of electronic and photonic IC with non-Gaussian correlated process variations," *IEEE Trans. Comput.-Aided Design Integr. Circuits Syst.*, vol. 39, no. 8, pp. 1649–1661, Aug. 2020.

[41] Y. Dodge and D. Commenges, *The Oxford Dictionary of Statistical Terms*. Oxford, U.K.: Oxford Univ. Press, 2006.

[42] H. Sheng and X. Wang, "Applying polynomial chaos expansion to assess probabilistic available delivery capability for distribution networks with renewables," *IEEE Trans. Power Syst.*, vol. 33, no. 6, pp. 6726–6735, Nov. 2018.

[43] G. Wang, H. Xin, D. Wu, P. Ju, and X. Jiang, "Data-driven arbitrary polynomial chaos-based probabilistic load flow considering correlated uncertainties," *IEEE Trans. Power Syst.*, vol. 34, no. 4, pp. 3274–3276, Jul. 2019.

Authorized licensed use limited to: to IEEExplore provided by University Libraries | Virginia Tech. Downloaded on May 20,2021 at 19:45:54 UTC from IEEE Xplore. Restrictions apply.

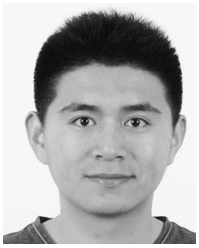

Yijun Xu (Member, IEEE) received the Ph.D. degree from the Bradley Department of Electrical and Computer Engineering, Virginia Tech, Falls Church, VA, USA, on December 2018.

He is currently a Research Assistant Professor with Virginia Tech, where he was a a Postdoctoral Associate with Virginia Tech from 2019 to 2020. He did the computation internship with Lawrence Livermore National Laboratory, Livermore, CA, USA, and a power engineer internship at ETAP—Operation Technology, Inc., Irvine, CA, USA, in 2018 and 2015, respectively. His research interests include power system uncertainty quantification, uncertainty inversion, and decision-making under uncertainty. He is currently serving as an Associate Editor of the *IET Generation, Transmission & Distribution*. He is the Co-Chair of the IEEE Task Force on Power System Uncertainty Quantification and Uncertainty-Aware Decision-Making.

Mert Korkali (Senior Member, IEEE) received the Ph.D. degree in electrical engineering from Northeastern University, Boston, MA, USA, in 2013.

He is currently a Research Staff Member with Lawrence Livermore National Laboratory, Livermore, CA, USA. From 2013 to 2014, he was a Postdoctoral Research Associate with the University of Vermont, Burlington, VT, USA. His current research interests lie at the broad interface of robust state estimation and fault location in power systems, extreme event modeling, cascading failures, uncertainty quantification, and probabilistic grid planning. He is the Co-chair of the IEEE Task Force on Standard Test Cases for Power System State Estimation and the Secretary of the IEEE Task Force on Power System Uncertainty Quantification and Uncertainty-Aware Decision-Making. He is currently serving as an Editor of the IEEE OPEN ACCESS JOURNAL OF POWER AND ENERGY and of the IEEE POWER ENGINEERING LETTERS, and an Associate Editor of *Journal of Modern Power Systems and Clean Energy*.

Lamine Mili (Life Fellow, IEEE) received the Ph.D. degree from the University of Liège, Belgium, in 1987.

He is a Professor of Electrical and Computer Engineering, Virginia Tech, Blacksburg. He has five years of industrial experience with the Tunisian electric utility, STEG, where he worked with the Planning Department from 1976 to 1979, and then with the Test and Meter Laboratory from 1979 to 1981. He was a Visiting Professor with the Swiss Federal Institute of Technology, Lausanne, the Grenoble Institute of Technology, the École Supérieure D'électricité, France, and the École Polytechnique de Tunisie, Tunisia, and did consulting work for the French Power Transmission company, RTE. His research has focused on power system planning for enhanced resiliency and sustainability, risk management of complex systems to catastrophic failures, robust estimation and control, nonlinear dynamics, and bifurcation theory. He is a recipient of several awards, including the U.S. National Science Foundation (NSF) Research Initiation Award and the NSF Young Investigation Award. He is the Chairman of the IEEE Working Group on State Estimation Algorithms and the Chair of the IEEE Task Force on Power System Uncertainty Quantification and Uncertainty-Aware Decision-Making. He is the Co-Founder and Co-Editor of the *International Journal of Critical Infrastructure*.

Jaber Valinejad (Member, IEEE) is currently pursuing the Ph.D. degree with the Bradley Department of Electrical and Computer Engineering, Virginia Tech, Greater Washington, D.C., USA. He is also pursuing the M.Sc. degree with the Department of Computer Science, Virginia Tech. He is with an NSF-sponsored interdisciplinary disaster resilience Program. His current research interests include power systems, resilience and community resilience, cyber-physical—social systems and social computing, artificial intelligence, and learning.

Tao Chen (Member, IEEE) received the B.S. degree in electrical engineering from Anhui University, Hefei, China, in 2012, the M.S. degree in electrical engineering from the Tampere University of Technology, Tampere, Finland, in 2014, and the Ph.D. degree in electrical engineering from the University of Michigan—Dearborn, Dearborn, MI, USA, in 2018. He is currently a Lecturer with the School of Electrical Engineering, Southeast University, Nanjing, China. He was a Postdoctoral with Virginia Tech from 2018 to 2019. His research interests include machine learning applications in power system, demand side management, and electricity market.

Xiao Chen received the Ph.D. degree in applied mathematics from Florida State University, Tallahassee, FL, USA, in 2011. He is a Computational Scientist and a Project Leader with the Center for Applied Scientific Computing with Lawrence Livermore National Laboratory, Livermore, CA, USA. He works primarily on the development and application of advanced computational and statistical methods and techniques to power engineering, reservoir simulation, subsurface engineering, and seismic inversion. His research interests include uncertainty quantification, data assimilation, and machine learning.

Authorized licensed use limited to: to IEEExplore provided by University Libraries | Virginia Tech. Downloaded on May 20,2021 at 19:45:54 UTC from IEEE Xplore. Restrictions apply.